High-Resolution 3D Whole-Heart Coronary MRA: A Study on the Combination of Data Acquisition in Multiple Breath-Holds and 1D Residual Respiratory Motion Compensation

Christoph Forman[1,2], Davide Piccini [3,4], Robert Grimm[1], Jana Hutter[1,2], Joachim Hornegger[1,2], and Michael O. Zenge[5]

Affiliations:

1 Pattern Recognition Lab, Department of Computer Science, Friedrich-Alexander University of Erlangen-Nuremberg, Erlangen, Germany

2 Erlangen Graduate School in Advanced Optical Technologies (SAOT), Friedrich-Alexander University of Erlangen-Nuremberg, Erlangen, Germany

3 Advanced Clinical Imaging Technology, Siemens Healthcare H IM BM PI, Lausanne, Switzerland

4 Department of Radiology, University Hospital (CHUV) and University of Lausanne (UNIL) / Center for Biomedical Imaging (CIBM), Lausanne, Switzerland

5 MR Product Innovation & Definition, Healthcare Sector, Siemens AG, Erlangen, Germany

Notes:

Running Head: 3D Whole-Heart CMRA in Multiple Breath-Holds

Correspondence to: Christoph Forman,
Pattern Recognition Lab
(Department of Computer Science)
Friedrich-Alexander University of Erlangen-Nuremberg,
Martensstr. 3, D-91058 Erlangen, Germany.
E-mail: christoph.forman@cs.fau.de.
Phone: +49 9131 85 27775
Fax: +49 9131 303811

Word count:

Abstract:	196	Figures:	4
Manuscript:	ca. 4399	Tables:	1
		References:	35

Object To study a scan protocol for coronary MRA based on multiple breath-holds featuring 1D motion compensation and to compare the resulting image quality to a navigator-gated free-breathing acquisition. Image reconstruction was performed using L1 regularized iterative SENSE.
Materials and methods The effects of respiratory motion on the Cartesian sampling scheme were minimized by performing data acquisition in multiple breath-holds. During the scan, repetitive readouts through k-space center were used to detect and correct the respiratory displacement of the heart by exploiting the self-navigation principle in image reconstruction. In-vivo experiments were performed in 9 healthy volunteers and the resulting image quality was compared to a navigator-gated reference in terms of vessel length and sharpness.
Results Acquisition in breath-hold is an effective method to reduce the scan time by more than 30% compared to the navigator-gated reference. Although an equivalent mean image quality with respect to the reference was achieved with the proposed method, the 1D motion compensation did not work equally well in all cases.
Conclusion In general, the image quality scaled with the robustness of the motion compensation. Nevertheless, the featured setup provides a positive basis for future extension with more advanced motion compensation methods.

Key words: Coronary magnetic resonance angiography; Multiple breath-holds, Respiratory motion compensation; Compressed sensing.

INTRODUCTION

Coronary magnetic resonance angiography (CMRA) provides great potential as an alternative to conventional X-ray imaging for the diagnosis of e.g. coronary artery disease without the need for ionizing radiation. In CMRA, a fast way to examine the coronary vessels is provided by thin targeted slabs for each vessel [1]. Nevertheless, even for experienced operators the setup of each individual protocol is a tedious task. 3D whole-heart imaging [2, 3] has been proposed to improve the workflow of this examination. This method allows for a retrospective reformatting of the final volume and, thereby, to display the coronary vessels in arbitrary orientations.

However, the extended acquisition time required by a whole-heart acquisition makes a careful compensation of different types of motion indispensable in order to achieve a good image quality: 1) Cardiac motion during data acquisition can mostly be avoided by segmented data acquisition and triggering relative to the R-wave of an electrocardiogram. In this case, each segment is acquired within the resting phase of the heart in the cardiac cycle. 2) The effects of respiratory motion need to be addressed differently for the data acquisition in free-breathing or in breath-hold.

Acquisitions in free-breathing are ideally not limited in scan time by the ability of the subjects to hold their breath. This is especially beneficial for children or patients suffering from specific medical conditions who are not able to hold their breath for a long period of time during the MR examination. On the other hand, these approaches require respiratory motion compensation which introduces an additional expenditure to the data acquisition. Most commonly, respiratory motion is efficiently minimized by gating the scan to the same respiratory state with the use of a hemidiaphragmatic navigator [4, 5]. However, the acceptance rate of such navigator methods is in many cases less than 50%. As a result, the total scan time is extended significantly. This issue is even worse in the presence of irregular breathing patterns. In most cases, these extended acquisitions result in a degraded image quality in the reconstructed images. The concept of 1D self-navigation was recently introduced in combination with radial imaging [6, 7] to overcome these problems. In this approach, the position of the heart is directly calculated from readouts acquired in superior-inferior (SI) direction within every heartbeat and can be used for motion compensation. Thus, a scan time efficiency of 100% can be achieved. While 1D self-navigation is efficient to compensate for motion along the SI direction, motion of the heart in other directions [8] or other motion effects such as chest wall motion remain critical.

In contrast to the free-breathing approach, the acquisition in breath-hold provides a simple method to efficiently minimize the effects of motion on the acquired data. Promising results for cardiac imaging have been described in literature [9, 10, 11] and an extensive study [12] has been

performed to assess the breath-hold capability and patterns in patients. However, the duration of a single breath-hold is limited and thus requires a general speed-up of the data acquisition. Conventionally, a reduction of the total scan time is achieved by acquiring every n-th line in k-space. In this case, parallel imaging methods [13, 14] allow to reconstruct images free of artifacts if the input data of multiple radio frequency receiver coils is available. Further acceleration in data acquisition has been achieved with compressed sensing [15] and promising results were shown for CMRA in combination with a navigator [16]. Furthermore, non-Cartesian sampling such as radial [17] or spiral [18] trajectories have been proposed for fast acquisition. However, these sampling schemes are sensitive to hardware imperfections of the MR scanner, such as gradient delays [19, 20], which might also require an elaborate compensation during the image reconstruction. Radial phase encoding (RPE) [21] has been proposed as a combination of readouts on the Cartesian grid with a non-Cartesian sampling of the phase-encoding plane. This trajectory is robust to motion artifacts, but is computationally demanding in the case of iterative reconstruction as gridding [22] is involved in each iteration. The use of an increased sampling density at the low spatial frequencies in k-space has been shown to be beneficial for convergence rates and reconstruction errors of iterative reconstruction [23]. Variable-density radial view ordering [24] and the Cartesian spiral phyllotaxis sampling pattern [25] provide an extension to RPE featuring a variable-density sampling pattern on the Cartesian grid. Furthermore, recent results with random Cartesian sampling of the phase-encoding plane [26] show that incoherent Cartesian sampling seems to be a competitive alternative to non-Cartesian sampling. In this particular context, a recent publication [27] highlighted the improvements in image quality when the parallel imaging reconstruction was combined with compressed sensing. Although all the methods mentioned above allow the acceleration of the data acquisition, still multiple breath-holds are required to achieve sufficient k-space coverage for 3D whole-heart coronary MRA in high resolution. Therefore, the data of subsequent breath-holds need to be consistent to avoid residual artifacts. This is specifically important for Cartesian sampling because it is more sensitive to residual motion than radial acquisitions.

The purpose of the current work was to study a scan protocol based on multiple breath-holds featuring 1D motion compensation and to compare the resulting image quality with a navigator-gated free-breathing acquisition. In both cases, data acquisition was accelerated by sub-sampling the phase-encoding plane with the Cartesian spiral phyllotaxis pattern [25]. For image reconstruction L1 regularized iterative SENSE was applied. Data of multiple breath-holds were combined including 1D respiratory motion correction based on the self-navigation principle which promised to compensate for the residual offsets of the heart between breath-holds. MR imaging experi-

ments were performed in-vivo in 9 healthy volunteers and the acquired datasets were compared to navigator-gated reference images with identical parameters for the acquisition and the reconstruction.

MATERIALS AND METHODS

Data Acquisition in Breath-hold

The acquisition time during one breath-hold is limited and, in most cases, too short for ECG-triggered 3D whole-heart acquisition in high resolution. Therefore, the data acquisition was segmented over multiple breath-holds and heartbeats. For each breath-hold the phase-encoding plane was sampled using a variable-density Cartesian spiral phyllotaxis pattern. This pattern is similar to [28] and has proven to facilitate segmented data acquisition, e.g. in the end-diastolic phase of the cardiac cycle, as well as it provides smooth gradient waveforms to avoid eddy current effects in case of balanced steady-state free-precession (bSSFP) data acquisition. Equivalent to [21, 24], each segment in this trajectory starts with readouts near the center of k-space and ends at the high frequencies. An increased sampling density of the low spatial frequencies in k-space was achieved with an additional factor $d \in \mathbb{R}$ in the normalized formulation of the spiral phyllotaxis pattern:

$$r(n) = \left(\frac{n}{N_h \cdot N_s}\right)^{0.5+d} \qquad d > -0.5 \tag{1}$$

$$\varphi(n) = n \cdot \varphi_{\text{gold}} + \varphi_{\text{offset}}, \tag{2}$$

where the radius $r(n)$ is defined as a function of the sampling point $n = 1, 2, \ldots, (N_h \cdot N_s)$, which is normalized by the product of the number of heartbeats N_h and the amount of readouts N_s acquired within each segment. Increasing the exponent $0.5 + d$ results in an increased sampling density at the low spatial frequencies. For each sampling point, the polar angle $\varphi(n)$ is incremented by φ_{gold}, which is the golden angle of the full circumference. An additional angle φ_{offset} allows a rotation of the entire sampling pattern. The sampling points are interleaved to create the final trajectory. If N_h is any combination of Fibonacci numbers and is used for interleaving, then the trajectory for each segment results in minimum distances between consecutive readouts as shown in Figure 1. Intrinsically, successive segments are rotated by the golden angle. Finally, a nearest-neighbour interpolation is performed to map the 2D polar coordinates of the sample points specifying the start of each readout onto the Cartesian grid to avoid the time-consuming gridding step during

image reconstruction.

1D Residual Respiratory Motion Compensation

For the acquisition of a consistent set of data, the multiple-breath-hold procedure requires the examined subject to be able to stop his/her respiration repeatedly in the very same position. However, variations in the respiratory positions between breath-holds are common and to be expected. If uncorrected, these variations lead to respiratory motion artifacts that degrade the final image quality. The major component of respiratory motion on the heart is along the superior-inferior (SI) direction [29]. This is also expected for a potential offset of the heart in subsequent breath-holds. For the detection of these offsets, an additional readout going through k-space center and consistently oriented along the SI direction is acquired at the beginning of each data segment. The Fourier transform of these readouts are henceforth referred to as SI projections, as they represent the orthogonal projection of the imaging volume along the SI direction. Based on the SI projections respiratory self-navigation is performed as described in [7]. As mentioned in the same paper, bright sources of signal that can negatively influence the detection of the heart by self-navigation need to be reduced during data acquisition. Therefore, a saturation slab was placed on the anterior chest wall to suppress the bright signal of the chest [1]. Lateral signal, e.g. of the arms, is excluded with a sagittal slab excitation for the data acquisition. Hence, in contrast to non-selective 3D radial imaging a retrospective suppression of this signal is not required for self-navigation. The motion detection procedure consists of several steps: 1) To reduce unwanted static signal from the spine on the SI projections the spine coil array is excluded from further processing. 2) The SI projection is generated based on the Fourier transformed signal of all the elements of the body array coil and followed by a sum-of-squares combination. 3) The first SI projection of the first breath-hold was selected as a reference respiratory position. Only in this projection, a region covering the signal of the heart is automatically detected as described in [7]. 4) The SI displacement of all subsequent SI projections is estimated as the offset that maximizes the cross-correlation with respect to the region in the reference projection as detected in step 3. As an example, Figure 2 illustrates the detection of this SI displacement for three consecutive breath-holds. 5) The data of every acquired segment is then corrected to the reference by multiplication of the linear phase in k-space that corresponds to the respective offset computed in step 4. During the data acquisition, all SI projections and a graphical overlay indicating the detected respiratory offset were displayed on the monitor at the MR control room.

Image Reconstruction

The acquired data were reconstructed using a regularized iterative SENSE reconstruction, which optimized the following objective function:

$$f(x) = \underset{\mathbf{x}}{\operatorname{argmin}} \|\mathbf{A}\mathbf{x} - \mathbf{y}\|_2^2 + \lambda R(\mathbf{x}). \tag{3}$$

The first part of the cost function optimizes the data fidelity of the reconstructed image $\mathbf{x} \in \mathbb{C}^{N_x N_y N_z}$ with respect to the measured data $\mathbf{y} \in \mathbb{C}^{N_k N_c}$, where N_k is the number of acquired k-space samples and N_c are the used coil elements. Following the notation of [13], the entries of the system matrix $\mathbf{A} \in \mathbb{C}^{N_k N_c \times N_x N_y N_z}$ are defined by

$$\mathbf{A}_{(\gamma,\kappa),\rho} = e^{ik_\kappa r_\rho} c_\gamma(r_\rho), \tag{4}$$

where r_ρ is the position of the ρ-th voxel in image domain, k_κ denotes the κ-th frequency and c_γ is the known spatial coil sensitivity of the γ-th coil element. In this work, the additional regularization term $R(x)$ is represented by the 3D total variation (TV) norm [30], that likewise applies a penalty on the incoherent artifacts in the final image. Using this regularization term, the optimization problem results in a compressed sensing reconstruction [15]. The described objective function is solved using the limited-memory Broyden-Fletcher-Goldfarb-Shanno (L-BFGS) method [31]. By applying the Fourier transform in the fully sampled readout direction, the data fidelity term can be divided into multiple 2D reconstruction problems, which facilitates a parallel processing.

MR Experiments

In-vivo experiments were performed in 9 healthy volunteers on a 1.5 T clinical MR scanner (MAGNETOM Aera, Siemens AG, Healthcare Sector, Erlangen, Germany), with software release syngo MR D11. Signal reception was performed using one 18-channel body array coil and 8 elements of the spine array coil. All measurements were ECG-triggered. The individual trigger delay to the subject-specific cardiac resting period was adjusted using a two-dimensional cine scan with axial slice orientation performed prior to the coronary acquisition. The whole-heart imaging volume was placed in sagittal slice orientation with the blood pool of the heart positioned in the center of the FOV. 3D volume-selective, T2-prepared, fat-saturated bSSFP imaging was performed for both navigator-gated and the proposed breath-hold acquisitions with the following parameters: TR/TE 4.0/2.0 ms, radio frequency excitation angle 90°, FOV $270 \times 270 \times 167\,\mathrm{mm}^3$, acquired

matrix $256 \times 218 \times 150$, reconstructed matrix $256 \times 256 \times 176$, slice oversampling 22%, voxel size $1.05\,\mathrm{mm}^3$ and a receiver bandwidth of 849 Hz/Px. For the multiple-breath-hold approach, the data acquisition was segmented over 8 breath-holds. The sampling pattern for each breath-hold was generated with $N_h = 21$ heartbeats, and $N_s = 30$ readouts, which were acquired during the end-diastolic phase of the cardiac cycle. At the beginning of the acquisition of each heartbeat, an additional SI readout for respiratory motion detection was acquired. The combination of the sampling density factor and the rotation of the sampling pattern between breath-holds with the nearest-neighbor interpolation results in some k-space samples that are acquired more than once. This effect is observed at the low spatial frequencies in k-space and the amount of duplicate readouts increased with an improved sampling density in this region of k-space. Hence, the sampling density factor $d = 0.2$ and $\varphi_{\mathrm{offset}} = 0.1$ were heuristically set to avoid such duplicate readouts as far as possible. In the combined dataset, the redundant readouts replaced previously acquired data at the same k-space location. Nevertheless, the net acceleration factor of 6.5 was determined by the quotient of the total number of acquired readouts $N_h \times N_s$ and the size of the acquisition matrix in the phase-encoding plane. A 20 s resting time was added between the breath-holds to let the volunteer recover from the previous acquisition. The navigator-gated acquisition was performed using an acceptance window of 5 mm placed in end-expiration. Slice tracking with a fixed correlation factor of 0.6 [29] was activated. Navigator-gated data acquisition was performed in one single scan implementing the very same sampling scheme used in the proposed method. The coil sensitivities were obtained from an initial reference scan. In all cases, no data acquisition was performed within the first heartbeat to minimize artifacts from signal oscillations in the first SI projection which was used as the reference.

The acquired data was reconstructed with $\lambda = 0.015$ for the TV regularization for all scans in multiple breath-holds as well as using navigator-gating. In all cases, the reconstruction was terminated after a predefined number of 5 iterations. Preliminary offline studies indicated that after this number of iterations no considerable improvement of the data fidelity has been achieved. Both the respiratory motion detection and the compressed sensing image reconstruction were fully integrated into the software of the MR scanner.

Data Analysis

For the evaluation of the scan efficiency the average acquisition time of all breath-hold scans was compared to the average scan time of the coronary scans with the navigator-gated protocol. The analysis of the data consistency in the combined dataset obtained with acquisition in multiple breath-holds required the differentiation between residual motion intra and inter breath-holds.

This was performed by a retrospective evaluation of the detected offsets in the SI projections. For the evaluation of data consistency within each breath-hold the standard deviation of the detected offsets was estimated. In case of a perfect breath-hold this estimate would be 0, while it would increase when the volunteer was not able to hold the breath. The general ability of each volunteer to hold the breath during the experiment was determined by averaging the estimates of all breath-holds. The range of the detected offsets describes the distribution of the position of the heart during the entire examination and, thus, delineates the reproducibility of breath-holds.

For the assessment of image quality, vessel length and sharpness were compared for both methods. A centerline was manually segmented for both the right coronary artery (RCA) and the left anterior descending artery (LAD) in the 3D isotropic volumes using CoronaViz (Work-in-Progress software, Siemens Corporate Research, Princeton, NJ, USA). The vessel length was measured by the length of the centerlines. For the quantitative assessment of vessel sharpness, up to 41 measurement points were placed over the first 40 mm of each centerline with a spacing of 1 mm. At each measurement point, 5 cross-sections with an angular spacing of 36° were defined perpendicular to the segmented centerline. On each cross-section, the sharpness was evaluated by the inverse of the average distance between 20% and 80% of the maximum signal intensity on both sides as described in [32]. The resulting values for each method and vessel were averaged to provide a quantitative measure of image quality. A paired two-tailed Student's t-test was performed in all obtained results to evaluate statistical significance. P-values of 0.05 or less were considered as statistically significant.

RESULTS

Whole-heart navigator-gated acquisitions as well as those performed with the multiple-breath-hold protocol were successful in all volunteers. The acquisition time of a single breath-hold was dependent on the subject's individual heart-rate and required 26.2 ± 2.3 s. Including the pauses in-between the scans, the examinations in breath-hold resulted in an average total scan time of 5.8 ± 0.3 min. The navigator-gated reference scans performed with an average acceptance rate of $43.7 \pm 11\%$, which prolonged the acquisition time to 8.6 ± 4.1 min. Using the breath-hold protocol, the scan time was reduced to 67% of the required time for the navigator-gated reference scan. However, with $p = 0.06$, this difference was not statistically significant. Nevertheless, the limitations of navigator-gating became apparent in the experiment with subject 2 as the irregular breathing pattern of this subject led to a total scan time of 19 min. For both types of the acquisition, the image reconstruction time of each examination was, on average, 52.4 ± 4.9 s. The

optimization finished with an improvement of the cost function in the last iteration of less than 1% relative to the L_2-norm of the acquired data. This confirms the observations of the preliminary study.

Figure 3 illustrates the evaluation of the respiratory offsets as detected in the SI projections of the breath-hold scans. The mean intra-breath-hold displacement of the heart was measured with a standard deviation of 0.7 ± 0.4 mm. The largest mean standard deviation was measured with 1.2 mm for subject 8. The range of the inter-breath-hold respiratory displacements of the heart was minimal with 4.2 mm for subject 9, maximal with 12.6 mm for subject 8 and was on average 8.8 ± 2.8 mm. Subjects 4 and 9 were able to reproduce the same position for almost every breath-hold, and thereby provide an example of high spatial consistency. The largest distribution of breath-hold positions over a wide range was observed in the experiment with subject 5, where the heart was detected at 5 different positions out of 8 breath-holds. Although the detected offsets were corrected during image reconstruction, the final image exhibits artifacts similar to uncompensated respiratory motion in a free-breathing acquisition.

The quantitative evaluation of the reconstructed volumes is provided in Table 1 for each of the 9 volunteers. On average, a vessel length of 131.0 ± 30.4 mm for the RCA and 113.2 ± 18.4 mm for the LAD was segmented on navigator-gated data. In the breath-hold data, manual segmentation resulted in a mean vessel length of 101.2 ± 41.3 mm and 99.8 ± 40.5 mm, respectively. Note that residual artifacts in the experiment with subject 5 allowed only a segmentation of the coronary arteries over a length of 30 mm for the RCA and 26 mm for the LAD in the corresponding volumes. Figure 4 shows the reformatted images of the RCA and LAD for both acquisitions side-by-side. Finally, the evaluation of the vessel sharpness along the segmented centerlines resulted in similar estimates for the RCA of 0.361 ± 0.060 in the datasets acquired in breath-hold compared to 0.371 ± 0.055 of the navigator-gated reference and for the LAD of 0.380 ± 0.033 and 0.393 ± 0.037, respectively. Overall, the assessment of the vessel length ($p > 0.08$) and sharpness ($p > 0.31$) revealed no significant difference in image quality for both methods.

DISCUSSION

In the current work, the competitive methods were highly accelerated using compressed sensing. But one of the major advantages of the multiple-breath-hold approach over navigator-gated free-breathing acquisitions is that the scan time is only dependent on the subject's heart rate and the recovery time between breath-holds. Thereby, a total scan time with a small standard deviation was achieved in the experiments using the multiple-breath-hold method. This renders

the total acquisition time predictable, which is beneficial for the planning of an MR examination. In contrast to this, the scan time of the navigator-gated protocol can be significantly prolonged by an irregular respiration of the subject during the data acquisition. In the current work, this was particularly the case with the navigator reference scan of subject 2 featuring a scan efficiency of only 22%. Typically, also the image quality is negatively affected in such cases.

While navigator-gated free-breathing acquisitions intrinsically provide consistent data, specific care was required in case of independent acquisitions in breath-hold. In all experiments, the mean intra-breath-hold offset of the heart was small compared to the maximum allowed displacement in the navigator-gated scans, even when such displacement was scaled using the correlation coefficient published in [29]. In the majority of cases it was even below the acquired resolution. In terms of breath-hold capability, subject 8 was identified as an outlier, who was not able to hold his breath efficiently. For this subject the 1D motion compensation failed to correct for the effects of an irregular breath-hold pattern.

Nevertheless, the inter-breath-hold displacement, which on average exceeded the scaled acceptance window of the navigator almost by a factor of 3, had a dominating effect on the image quality. The detected respiratory offsets and the corresponding image quality in the reconstructed images imply that the 1D motion correction did not work equally well in all cases. For example, in subject 4 the intra- and inter-breath-hold displacements were in a range similar to the size of the navigator acceptance window, but the image quality was evidently better for the multiple-breath-hold method. In this case, the SI correction seemed to work properly. Even in the presence of large inter-breath-hold displacements the motion compensation proved to be efficient as seen in subject 2. Nevertheless, the correction was apparently ineffective in subject 5, that showed similar characteristics in the SI projections as subject 2. Here, the quantitative and qualitative image quality was considerably degraded compared to the navigator-gated reference. A possible explanation for this effect would be the limitation of the respiratory motion detection on basis of the 1D SI projections. In such cases, respiratory motion orthogonal to the SI direction reduced the efficiency of the compensation. While this compensation method seemed to be effective for small displacements, the consequences of this limitation become evident in the presence of large displacements and render it insufficient in combination with the motion-sensitive Cartesian sampling.

Recent publications promise to overcome these limitations by an extension of 1D self-navigation to 2D navigator images to detect two-dimensional motion [33] or establish a 3D non-rigid motion model [34]. Alternatively, 1D self-navigation has been efficiently used as input to minimize respira-

tory motion during weighted iterative reconstruction in CMRA [35]. Such methods can be applied to acquisitions in free-breathing as well as in breath-hold. Furthermore, the featured setup is already well prepared to integrate more sophisticated motion compensation. The sampling pattern, for example, supports the reconstruction of sub-images which might feed into non-rigid registration. This would allow to compensate the residual motion while overcoming the limitations of the SI projection.

The iterative reconstruction was terminated with a small improvement in the last iteration. This implies that a convergence was reached and the use of five iterations is sufficient for the minimization of equation 3. Furthermore, the use of an additional regularization during iterative reconstruction always leads to a tradeoff between reducing artifacts from the incoherent sampling in k-space and preserving small anatomical structures. In the resulting images, the coronary arteries were well depicted, while the iterative reconstruction was efficiently able to reduce the undersampling artifacts. Hence, it seems that a balance between both aspects was found with the current regularization. In addition, the parameters were fixed during the experiment and no subject specific variation of the regularization was observed in the resulting images. This suggests that this parameter can potentially also kept fixed for a routine use of the proposed method. Nevertheless, more advanced methods, that e.g. exploit the spatial similarities learned from the images during reconstruction [26], promise to be superior to a TV regularized reconstruction. However, the evaluation of these methods in combination with the proposed incoherent sampling pattern will be subject of future work. Thereby, the improved image quality of such methods might potentially facilitate a further acceleration of the data acquisition.

One limitation of this study was that only a small number of healthy volunteers were examined. Furthermore, the breath-hold durations that were utilized for the data acquisition were rather long and might be too demanding for a patient population suffering from cardiovascular diseases. However, the study of Jahnke et al. [12] suggests that such breath-hold times are possible at least in a feasibility study like the current work. The results show that, with only one exception, all subjects were able to hold breath sufficiently over this long period of time. The resulting image quality in the experiments featuring a high data consistency show that holding breath is a suitable method to reduce respiratory motion. Additionally, artifacts due to undersampling were efficiently reduced in these images. This implies that a further acceleration of the data acquisition might be feasible. Furthermore, the acquisition parameters in the current study were fixed to provide a consistent comparison of both methods over all subjects. However, the closed form solution of the sampling pattern also permits for individual adjustments of the scan parameters.

Thereby, the number of shots can be specifically adapted to account for the breath-hold capability of the subject. In this case, further optimizations of the sampling pattern might be desirable. This includes an improvement of the interpolation of sample points on the Cartesian grid to avoid redundant readouts in the region of the low frequencies in k-space and maintain a full scan efficiency.

CONCLUSION

The proposed acquisition in multiple breath-holds with SI motion compensation proved to be effective in reducing the scan time by more than 30% compared to the navigator-gated reference. Although the average vessel length and sharpness were statistically equivalent for both approaches, the achieved image quality substantially scaled with the robustness of the motion compensation. More advanced compensation methods will be evaluated in future work, which promise to achieve the required robustness for the use in clinical routine.

ACKNOWLEDGMENTS

The authors gratefully acknowledge funding of the Erlangen Graduate School in Advanced Optical Technologies (SAOT) by the German Research Foundation (DFG) in the framework of the German excellence initiative.

REFERENCES

[1] Stuber M, Botnar RM, Danias PG, Sodickson DK, Kissinger KV, Van Cauteren M, De Becker J, Manning WJ (1999) Double-oblique free-breathing high resolution three-dimensional coronary magnetic resonance angiography. J Am Coll Cardiol 34:524531.

[2] Weber OM, Martin AJ, Higgins CB (2003) Whole-Heart Steady-State Free Precession Coronary Artery Magnetic Resonance Angiography. Magn Reson Med 50:1223–1228.

[3] Hauser TH, Manning WJ (2008) The Promise of Whole-Heart Coronary MRI. Current Cardiology Reports 10:46–50.

[4] Danias PG, McConnell MV, Khasgiwala VC, Chuang ML, Edelman RR, Manning WJ (1997) Prospective Navigator Correction of Image Position for Coronary MR Angiography. Radiology 203:733–736.

[5] Stuber M, Botnar RM, Danias PG, Kissinger KV, Manning WJ (1999) Submillimeter Three-dimensional Coronary MR Angiography with Real-time Navigator Correction: Comparison of Navigator Locations. Radiology 212:579–587.

[6] Stehning C, Börnert P, Nehrke K, Eggers H, Stuber M (2005) Free-Breathing Whole-Heart Coronary MRA With 3D Radial SSFP and Self-Navigated Image Reconstruction. Magn Reson Med 54:476–480.

[7] Piccini D, Littmann A, Nielles-Vallespin S, Zenge MO (2012) Respiratory Self-Navigation for Whole-Heart Bright-Blood Coronary MRI: Methods for Robust Isolation and Automatic Segmentation of the Blood Pool. Magn Reson Med 68:571–579.

[8] Nehrke K, Börnert P, Manke P, Böck JC (2001) Free-breathing Cardiac MR Imaging: Study of Implications of Respiratory Motion – Initial Results. Radiology 220:810–815.

[9] Manning WJ, Li W, Boyle NG, Edelman RR (1993) Fat-suppressed breath-hold magnetic reso- nance coronary angiography. Circulation 87:94–104.

[10] Peters DC, Ennis DB, Rohatgi P, Syed MA, McVeigh ER, Arai AE (2004) 3D Breath-Held Cardiac Function With Projection Reconstruction in Steady State Free Precession Validated Using 2D Cine MRI. JMRI 20:411–416.

[11] Niendorf T, Hardy CJ, Giaquinto RO, Gross P, Cline HE, Zhu Y, Kenwood G, Cohen S, Grant AK, Joshi S, Rofsky NM, Sodickson DK (2006) Toward Single Breath-Hold Whole-Heart

Coverage Coronary MRA Using Highly Accelerated Parallel Imaging With a 32-Channel MR System. Magn Reson Med 56:167–176.

[12] Jahnke C, Paetsch I, Achenbach S, Schnackenburg B, Gebker R, Fleck E, Nagel E (2006) Coronary MR Imaging: Breath-hold Capability and Patterns, Coronary Artery Rest Periods, and β-Blocker Use. Radiology 239(1):71–78.

[13] Pruessmann KP, Weiger M, Scheidegger MB, Boesiger P (1999) SENSE: Sensitivity Encoding for Fast MRI. Magn Reson Med 42:952–962.

[14] Griswold MA, Jakob PM, Heidemann RM, Nittka M, Jellus V, Wang J, Kiefer B, Haase A (2002) Generalized Autocalibrating Partially Parallel Acquisitions (GRAPPA). Magn Reson Med 47:1202–1210.

[15] Lustig M, Donoho D, Pauly JM (2007) Sparse MRI: The Application of Compressed Sensing for Rapid MR Imaging. Magn Reson Med 58:1182–1195.

[16] Moghari MH, Akçakaya M, O'Connor A, Basha TA, Casanova M, Stanton D, Goepfert L, Kissinger KV, Goddu B, Chuang ML, Tarokh V, Manning WJ, Nezafat R (2011) Compressed-Sensing Motion Compensation (CosMo): A Joint Prospective-Retrospective Respiratory Navigator for Coronary MRI. Magn Reson Med 66:1674–1681.

[17] Block KT, Uecker M, Frahm J (2007) Undersampled Radial MRI with Multiple Coils. Iterative Image Reconstruction Using a Total Variation Constraint. Magn Reson Med 57:1086–1098.

[18] Santos JM, Cunningham CH, Lustig M, Hargreaves BA, Hu BS, Nishimura DG, Pauly JM (2006) Single Breath-Hold Whole-Heart MRA Using Variable-Density Spirals at 3T. Magn Reson Med 55:371–379.

[19] Peters DC, Derbyshire JA, McVeigh ER (2003) Centering the projection reconstruction trajectory: reducing gradient delay errors. Magn Reson Med 50(1):1–6.

[20] Block KT, Uecker M(2011) Simple Method for Adaptive Gradient-Delay Compensation in Radial MRI. In: Proceedings of the 19th scientific meeting, International Society for Magnetic Resonance in Medicine, Montreal, Canada, p. 2816.

[21] Boubertakh R, Prieto C, Batchelor PG, Uribe S, Atkinson D, Eggers H, Sørensen TS, Hansen MS, Razavi RS, Schaeffter T (2009) Whole-Heart Imaging Using Undersampled Radial Phase

Encoding (RPE) and Iterative Sensitivity Encoding (SENSE) Reconstruction. Magn Reson Med 62:1331–1337.

[22] Jackson JI, Meyer CH, Nishimura DG, Macovski A (1991) Selection of a Convolution Function for Fourier Inversion Using Gridding. IEEE Trans Med Imaging 10:473–478.

[23] Doneva M, Eggers H, Börnert P(2012) CS-SENSE or Denoised SENSE: The Influence of Irregular Sampling in l1 Regularized SENSE Reconstruction. In: Proceedings of the 20th scientific meeting, International Society for Magnetic Resonance in Medicine, Melbourne, Australia, p. 2240.

[24] Cheng JY, Uecker M, Alley MT, Vasanawala SS, Pauly JM, Lustig M(2013) Free-Breathing Pediatric Imaging with Nonrigid Motion Correction and Parallel Imaging. In: Proceedings of the 21th scientific meeting, International Society for Magnetic Resonance in Medicine, Salt Lake City, UT, USA, p. 1506.

[25] Vogel H (1979) A Better Way to Construct the Sunflower Head. Math Biosci 44:179189.

[26] Akçakaya M, Basha TA, Chan RH, Rayatzadeh H, Kissinger KV, Goddu B, Goepfert LA, Manning WJ, Nezafat R (2012) Accelerated Contrast-Enhanced Whole-Heart Coronary MRI Using Low-Dimensional-Structure Self-Learning and Thresholding. Magn Reson Med 67:1434–1443.

[27] Vasanawala SS, Alley MT, Hargreaves BA, Barth RA, Pauly JM, Lustig M (2010) Improved Pediatic MR Imaging with Compressed Sensing. Radiology 256(2):607–616.

[28] Piccini D, Littmann A, Nielles-Vallespin S, Zenge MO (2011) Spiral Phyllotaxis: The Natural Way to Construct a 3D Radial Trajectory in MRI. Magn Reson Med 66:1049–1056.

[29] Wang Y, Riederer SJ, Ehman RL (1995) Respiratory Motion of the Heart: Kinematics and the Implications for the Spatial Resolution in Coronary Imaging. Magn Reson Med 33:713–719.

[30] Rudin LI, Osher S, Fatemi E (1992) Nonlinear total variation based noise removal algorithms. Physica D 60:259268.

[31] Nocedal J (1980) Updating Quasi-Newton Matrices with Limited Storage. Math. Comp. 35:773–782.

[32] Li D, Carr JC, Shea SM, Zheng J, Deshpande VS, Wielopolski PA, Finn JP (2001) Coronary Arteries: Magnetization-prepared Contrast-enhanced Three-dimensional Volume-targeted Breath-hold MR Angiography. Radiology 219:270–277.

[33] Henningsson M, Smink J, Razavi R, Botnar RM (2013) Prospective Respiratory Motion Correction for Coronary MR Angiography Using a 2D Image Navigator. Magn Reson Med 69:486–494.

[34] Schmidt JFM, Buehrer M, Boesiger P, Kozerke S (2011) Nonrigid Retrospective Respiratory Motion Correction in Whole-Heart Coronary MRA. Magn Reson Med 66:1541–1549.

[35] Forman C, Piccini D, Hutter J, Grimm R, Hornegger J, Zenge MO(2012) Minimization of Respiratory Motion Artifacts for Whole-Heart Coronary MRI: A Combination of Self-navigation and Weighted Compressed Sensing Reconstruction. In: Proceedings of the 20th scientific meeting, International Society for Magnetic Resonance in Medicine, Melbourne, Australia, p. 1160.

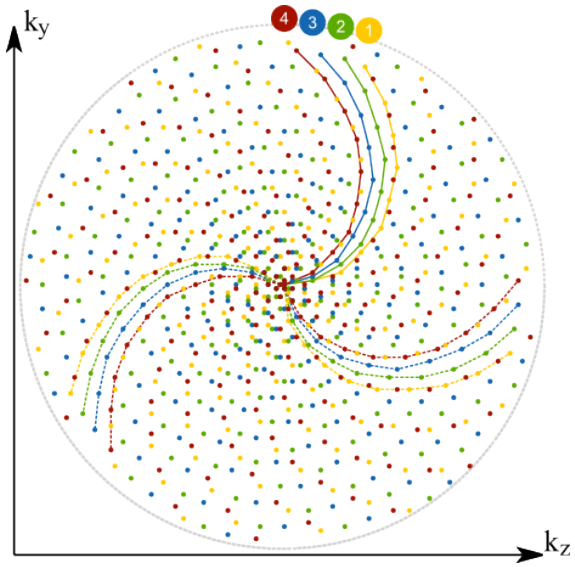

FIG. 1: Graphical representation of the spiral phyllotaxis pattern for the acquisition of 4 breath-holds. The pattern was generated only for the sampling of the first breath-hold with 21 segments containing 10 readouts each. Then, the sampling pattern was rotated by 0.1 radians for all successive breath-holds to ensure a homogeneous distribution of readouts for all breath-holds and to avoid re-sampling of redundant k-space lines. While each point represents the origin of a readout in the phase encoding plane, data of separate breath-holds are coded in different colors.

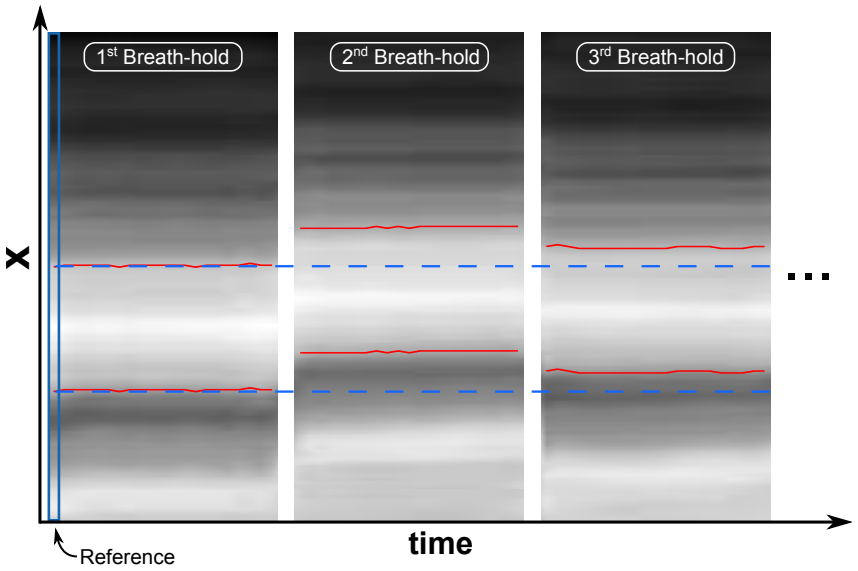

FIG. 2: Plot showing the acquired SI projections of three consecutive breath-holds: The first SI projection of the first breath-hold serves as a reference for the respiratory motion detection. In this projection the heart is segmented as proposed in [7], which is indicated by the dotted lines. Then, the SI displacement intra- and inter-breath-holds is estimated as the offset that maximizes the cross-correlation with respect to the region in the reference projection. These offsets are visualized by the red lines.

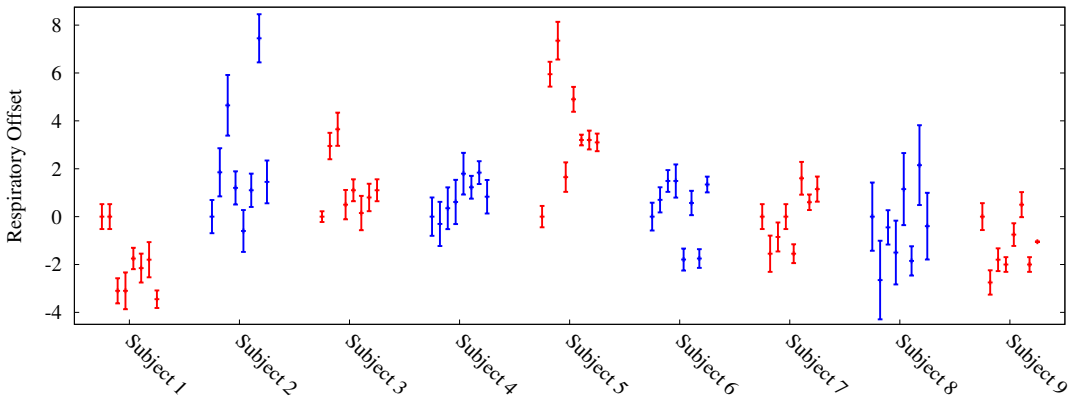

FIG. 3: Evaluation of the respiratory offsets as detected in the SI projections. The error bars show the mean value and the standard deviation of the estimated offsets in the SI projections for each acquisition in breath-hold. With an average standard deviation of 1.2 mm, subject 8 was identified as an outlier, who was able to hold breath less efficiently. Major challenges arise when it comes to the reproducibility of breath-holds to obtain a consistent dataset: Subjects 2 and 5 show large offsets between individual breath-holds.

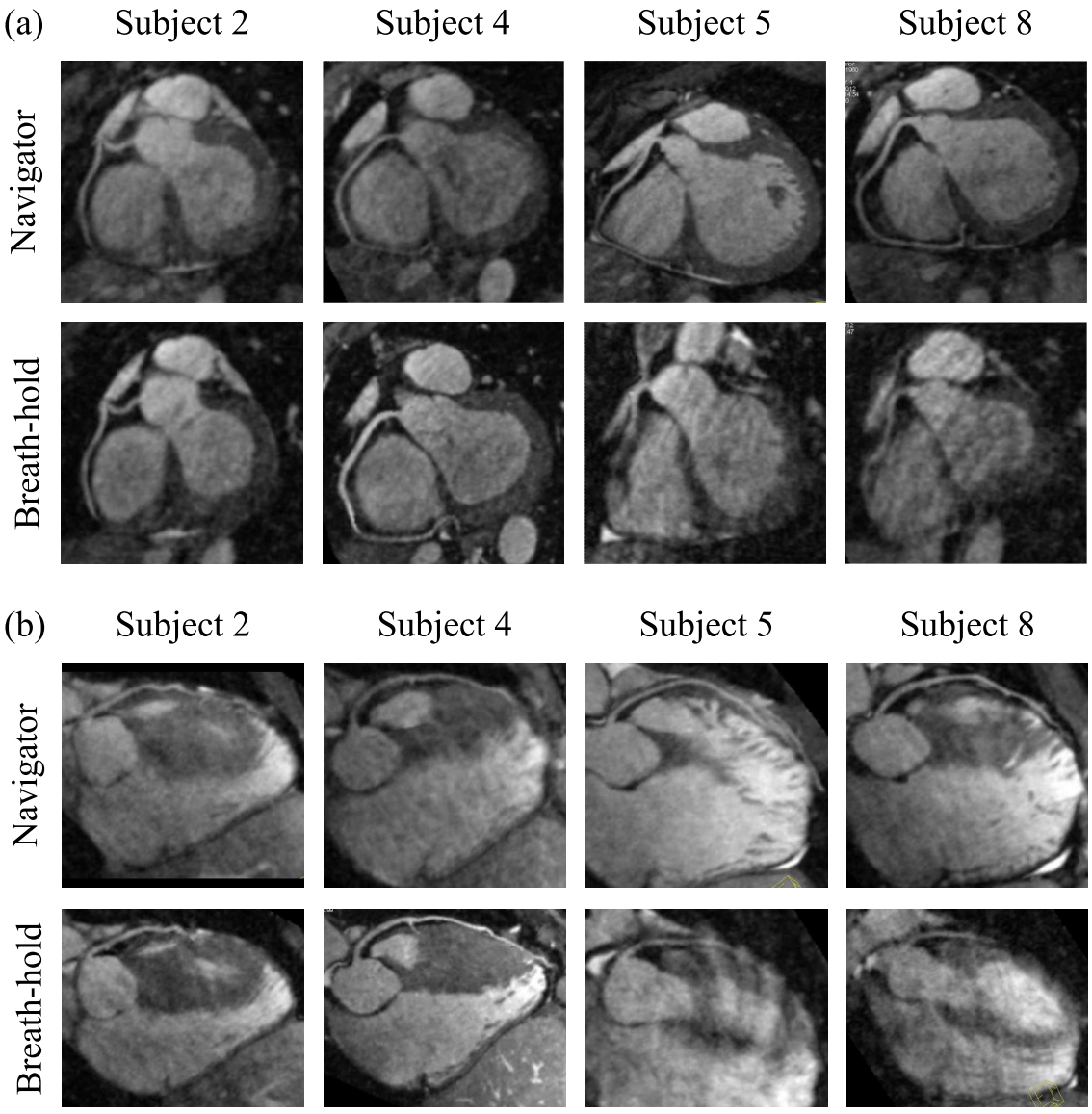

FIG. 4: Results of 4 selected volunteers, reformatted images of the *(a)* RCA and *(b)* LAD. The navigator-gated reference is compared with the described multiple-breath-hold approach. Subjects 2 and 4 provide an example with an improvement in image quality of the proposed multiple-breath-hold method. However, the SI correction did not work equally well in all cases as seen in the corresponding image quality in the reconstructed volumes of subjects 5 and 8.

	Navigator						Breath-hold				
	$t_{A\,[s]}$	Eff.	l [mm]		Sharpness [mm^{-1}]		$t_{A\,[s]}$	l [mm]		Sharpness [mm^{-1}]	
			RCA	LAD	RCA	LAD		RCA	LAD	RCA	LAD
Subject 1	590	0.50	105	89	0.323	0.354	370	120	81	0.324	0.351
Subject 2	1141	0.22	97	84	0.313	0.374	376	100	83	0.324	0.382
Subject 3	493	0.41	82	107	0.479	0.452	319	77	113	0.479	0.444
Subject 4	488	0.48	140	120	0.432	0.368	351	156	161	0.443	0.417
Subject 5	431	0.49	132	113	0.398	0.454	352	30	26	0.300	0.376
Subject 6	257	0.58	136	108	0.363	0.395	331	84	106	0.362	0.387
Subject 7	368	0.53	155	132	0.343	0.363	352	98	132	0.347	0.344
Subject 8	495	0.39	169	131	0.356	0.389	335	82	66	0.335	0.351
Subject 9	453	0.49	163	135	0.335	0.385	362	164	130	0.339	0.370
Average	523.8	0.45	131.0	113.2	0.371	0.393	349.8	101.2	99.0	0.361	0.380

Table 1: Numerical results for the comparison between the acquisitions in multiple breath-holds and the navigator-gated reference.